

Hot Deformation Behavior of Ni80A Superalloy During Non-Isothermal Side Pressing

M. Seyed Salehi¹, N. Anjabin^{2*} and R. Mansoori³

¹Department of Materials Science and Engineering, K. N. Toosi University of Technology, Tehran, Iran

²Department of Materials Science and Engineering, School of Engineering, Shiraz University, Shiraz, Iran

³Research and Development Center, Turbine Machine Middle East Co., Tehran, Iran

Abstract: In the present study, the microstructural changes of a Nickel based superalloy Nimonic 80A during a non-isothermal deformation were studied. Therefore, microstructure evolution during hot side pressing test was predicted with combined methods of finite element analysis and processing map of the material. The predicted results were validated through experimental microstructural studies. The results show that the distribution of deformation parameters (i.e. strain, strain rate, and temperature) is non-uniform in the deformed samples. The severity of this non-uniformity depends on the amount of sample reduction. High reduction value at one step forging can cause flow localization and non-uniform dynamic recrystallization, which results the formation of adiabatic shear bands, while using the lower reduction value at each forging step, leads to more uniformly distribution of the deformation parameters and thus uniform the dynamic recrystallization with the stable flow. Hence the workability and microstructure of the Nimonic 80A alloy are mainly depends on the deformation path.

Keywords: Hot deformation, Nimonic 80A, Processing map, Microstructure, Finite element analysis

1. Introduction

Nimonic 80A is a wrought, age-hardenable nickel-based superalloy which is strengthened by the addition of titanium, aluminum and carbon that is developed for parts used in high temperature applications [1-3]. Nimonic 80A due to its specific material properties such as high strength at elevated temperatures was used for turbine blades in some industrial gas turbine engines [3, 4]. Turbine blade is one of the most important mechanical components of turbine engines. Hot forging is extensively used for producing these blades [5]. However, hot working of Nimonic alloys is difficult because of limited workability and presence of complex phase system in these alloys [1-2]. Moreover, complicated geometry of turbine blades causes inhomogeneous distribution of deformation parameters such as strain, strain rate and temperature. Deformation inhomogeneity is more critical when the hot forging is done in non-isothermal condition, due to large surface contact of deforming hot material with the cold die [6]. The deformation inhomogeneity may cause flow localization and shear band formation [6, 7]. The severity of these flow localization mainly depend on specimen preheat temperature, die temperature, and forging speed [6]. On the other side, weak workability and high flow stress at low temperatures and incipient melting at high temperatures results in relatively narrow allowable temperature ranges for deformation of these alloys [8]. However, non-isothermal forging due to both lower cost and higher production rate is still extensively used in the metal forming industry [9, 10].

Since mechanical properties of the hot deformed material greatly depend on homogeneity of microstructure, it is needed to predict the effects of hot deformation parameters on the final

microstructure. Therefore, it is very important to control the dynamic metallurgical phenomena occurring during the deformation such as recrystallization and recovery [2]. Processing maps, in which maps the power efficiency of the deformation of the material in a strain rate/temperature space, are very helpful tools for this purpose [11]. According to these maps, processing parameters should be designed to operate in the region identified as stable or the safe region of deformation.

In this research, in order to study the microstructure evolution during the non-isothermal hot deformation of Ni80A alloy, laboratory side pressing tests with different deformation paths have been performed on the samples with different thermo-mechanical histories. Side-pressing is a type of open die forging in which a long cylindrical specimen lies on the bottom die surface and presses material between two flat dies in such a way that the longitudinal axis of the specimen (cylinder axis) is parallel to the die surfaces. This test is used to empirically simulate the plane-strain deformation condition of turbine blade forging. The variation of deformation parameters such as strain, strain rate and temperature in the deforming material were predicted by the finite element analysis. The processing maps with instability criteria, along with optical microscopy investigations were used to study the microstructural changes during deformation.

2. Experimental Procedure

Cylindrical specimens of 14 mm diameter and 60 mm height were machined from the received commercially rolled bar of Ni80A alloy. Non-isothermal hot side-pressing tests were done on the preheated samples using a mechanical press of crank type with 40 nominal strokes per minute and 300 mm connecting rod length. The die made from H13 tool steel and was used at room temperature. In order to study the effects of thermo-mechanical parameters on the microstructure, four samples were considered as listed in Table 1. The samples were cut and the cross section of each sample was polished and etched with an aqueous solution containing picric acid and then studied via optical microscopy.

Table 1. Thermo-mechanical route of side-pressed samples.

Sample code	Description
A1	Preheated at 1175 °C, then 35 % reduction (final thickness: 9mm) and finally air-cooled.
A2	Preheated at 1175 °C, then 35 % reduction (final thickness: 9mm), then 5 minute heating at 1175°C and finally air-cooled.
A3	Preheated at 1175 °C, then 35 % reduction (final thickness: 9mm), then 5 minute heating at 1175°C, then 44% reduction (final thickness: 5mm) and finally air-cooled.
A4	Preheated at 1175 °C, then 64 % reduction (final thickness: 5mm) and finally air-cooled.

3. Modeling Approach

3.1. Processing map

During plastic deformation, most of the consumed energy dissipated as heat which cause to increase the temperature of the deforming material. The remained energy served for metallurgical phenomena inside the material such as dynamic recovery and dynamic recrystallization. The power dissipation characteristics of the material during the hot deformation can be related to microstructural changes [11]. The efficiency of power dissipation occurring through microstructural changes (the ratio of dissipated energy due to metallurgical changes (dissipater co-content) to maximum dissipater co-content) can be related to the strain rate sensitivity of the flow stress (m) by;

$$\eta = \frac{2m}{m+1} \quad (1)$$

Since the strain rate sensitivity parameter depends on strain rate and temperature, the power efficiency can be plotted as an iso-efficiency contour map onto the strain rate - temperature plane, which is called as processing map. In these maps, the flow instability parameter ξ is used to define a criterion for flow instability [11].

$$\xi = \frac{\partial(m/m+1)}{\partial \ln \dot{\epsilon}} + m \quad (2)$$

During deformation, different phenomena such as adiabatic shear banding and flow localization can cause flow instability. In this condition, the instability parameter ξ is negative. Processing condition should be designed to operate in the region of stable flow ($\xi > 0$). Hence this parameter can be used to determine the boundaries between safe and unsafe regions on a processing map [12]. These maps help to identify temperature-strain rate regions that are appropriate for hot working and also in avoiding the regions of flow instabilities (e.g. adiabatic shear bands or flow localization) [7, 12]. Processing map and distribution of instability parameter for Ni80A were calculated based on the flow stress of the alloy [13].

3.2. Side press modeling

Side pressing is a commonly used experimental test for simulating the flow behavior of materials during non-uniform deformation such as turbine blade forging [5]. In the present study, the FEM software, Deform 3D, was used to model the non-isothermal side pressing test. As such, the heat transfer analysis was performed for the transferring step of billet from the preheat furnace to pressing die, and a coupled thermo-mechanical analysis was performed for the pressing step. Convection coefficient of heat transfer to the air (h), and also emissivity coefficient of radiation (e) for thermal analysis were obtained by the curve fitting of the predicted temperature on the measured one by the inserted thermocouple. The predicted values for heat transfer coefficients are $h = 5 \text{ w/m}^2\text{k}$ and $e=0.85$. The material assumed to behave as a rigid-viscoplastic material in the deformation analysis, using a constitutive equation being as follows [2]:

$$\sigma = \frac{1}{\alpha} \sinh^{-1} \left(\left(\frac{Z}{A} \right)^{\frac{1}{n}} \right) \quad (3)$$

where α , A and n are material constants, which assumed to have the values $0.002 \frac{1}{\text{MPa}}$, 5.32 and $4.47 \times 10^{16} \text{ s}^{-1}$ respectively [2]. Z is the Zener-Holoman parameter $Z = \dot{\epsilon} \exp(Q_{\text{def}}/RT)$, and Q_{def} is the activation energy for hot deformation, taken to be 379.28 kJ/mol K [2]. Moreover, the friction factor between die and workpiece is taken to be 0.4 . For the pressing step, a mechanical press is selected due to its benefit in higher production rate, lower die chilling and availability. The ram velocity during pressing predicted by the model was shown in Fig. 1, for two deformation paths, single and double stork forgings.

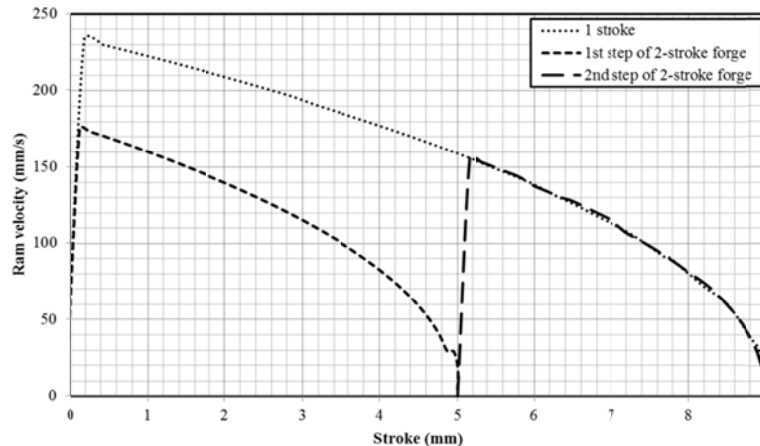


Fig. 1. Variation of ram velocity during single and double step forgings.

4. Result and Discussion

Figure 2 shows the distribution of effective strain, effective strain rate and temperature inside the cross-section of sample with 35% reduction in height, obtained by 3D FEM simulation. As shown in Fig. 2, the distribution of deformation parameters is not uniform, and an “X” pattern is formed. In this deformation pattern, the lowest temperature is found in the contact regions between die and work piece, due to heat transfer toward the die. Furthermore, regions near contact surfaces and free barreled surfaces have low values of strain and strain rate, while higher values of these deformation parameters are found in the X pattern. The strain rate gradient inside the cross section shows the tendency toward the formation of shear band or the localized plastic flow. The microstructure of deforming material highly depends on the distribution of deformation parameters, i.e. strain, strain rate and temperature. Therefore in this study, the deformation parameters distribution in different regions of deforming material cross section, as specified in Fig. 3 is considered along with the microstructural changes.

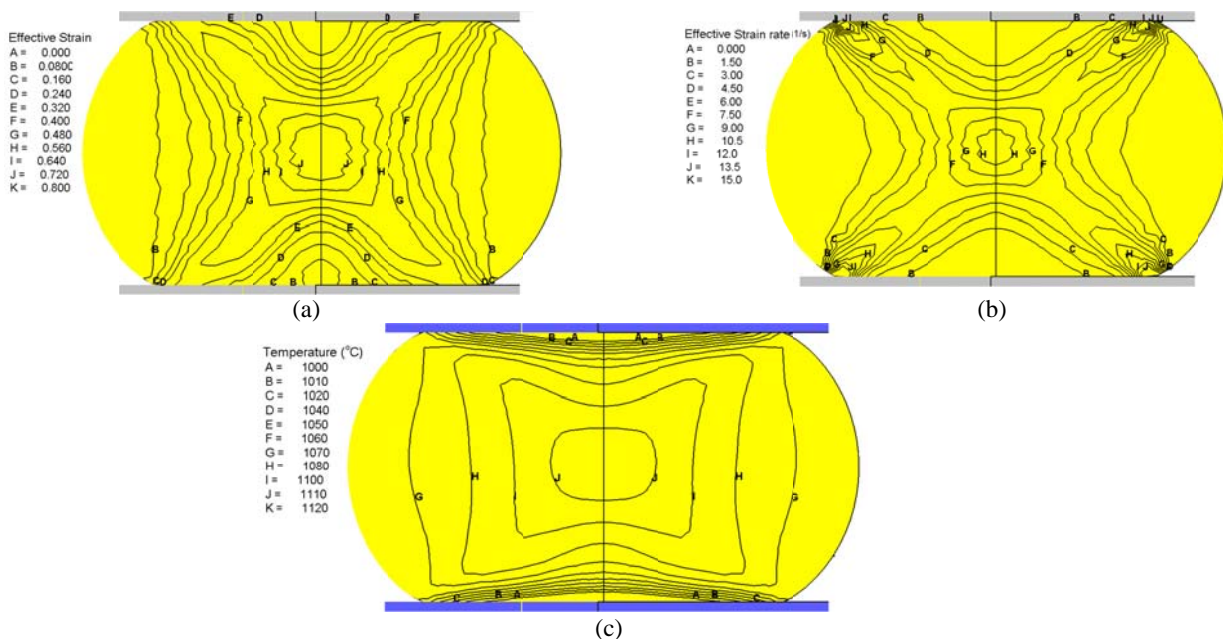


Fig. 2. Distribution of a) effective strain, b) effective strain rate and c) temperature of the cross section of sample with 35% reduction in height.

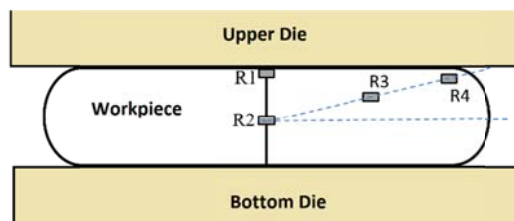


Fig. 3. Regions to be considered inside the cross section of deforming material.

4.1. Sample A1

From the FEM simulation results, in the sample A1, the equivalent strain of regions R1, R2, R3 and R4, are 0.03, 0.82, 0.31 and 0.08 respectively. Accordingly, the amount of strain in the regions R1 and R4 are lower than the critical strain needed for DRX formation, which is about 0.1 while regions R2 and R3 due to high stored energy from higher exposed strain are susceptible to DRX.

The microstructure of regions R1 and R4 are shown in Figs. 4 and 5 respectively. As shown in these figures, the accumulated plastic strain is not sufficient for DRX. In Fig. 5, the twins are deformed by the employed plastic strain. Fig. 6 shows the variation of strain rate vs. temperature for regions R2 and R3 of sample A1 inside the processing map of the alloy. The processing map was generated at the strain of 0.3 using the experimental flow stress data of Ni80A alloy reported by Prasad [11]. Three regions of I, II and III in Fig. 6, represent the flow instability, stable flow with no DRX and DRX domains, respectively. From Fig. 6, the instable flow appears in the top and top left corner domains, indicating that working flow instability phenomenon appears in above forming domains and should be avoided during practical forming. The domains with high power dissipation rate and no flow instability are appropriate for the forming (due to lower flow stress, stable flow and recrystallized equi-axed grains). According to Fig.6, as deformation proceeds, the temperature in regions R2 and R3 increase due to generation of heat during deformation. While strain rate increased during the early stages of deformation, it was decreased after reaching a maximum value. During side pressing as shown in Fig. 2, the strain rate distribution is non-uniform, and pattern "X" is formed in the material cross section, starting from part of the material that is in contact with die edges. At the beginning of deformation region R4 is not in contact with the die (far from X pattern leg). As the deformation proceeds, this region comes close in order to contact and the strain rate is increased. However, at higher reductions, region R4 goes far from X region legs and hence the strain rate is again decreased.

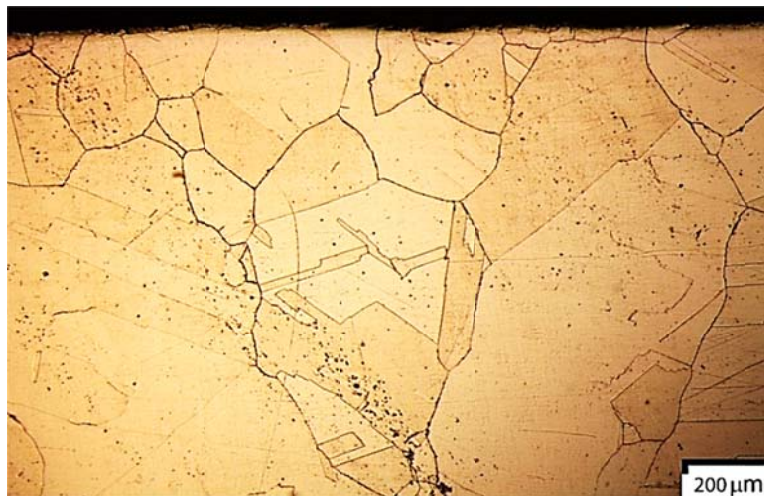


Fig. 4. Microstructure of region R1 of sample A1.

According to Fig. 6, although the temperature range in region R2 is suitable for DRX, strain rate is very high except in the last stages of deformation. Therefore, it is expected that the DRX is partially occurred in the deformed sample. The deformed microstructure of region R2 of sample A1 is shown in Fig. 7, which represents the partially recrystallized boundaries of highly elongated initial grains. The recrystallized grain size is very fine, which results from a very high strain rate.

As shown in Fig. 6, the thermo-mechanical condition for region R3 is on the boundary of DRX region. Therefore, this region is susceptible to undergoing DRX. The microstructure of region R3 is depicted in Fig. 8. Considering this microstructure, it is shown that DRX has happened in the most of grains in the early stages of deformation and further straining causes the recrystallized grains to be elongated in the flow direction. This condition is appropriate for second stage DRX by necklace mechanism. The presence of fine grains along the relatively elongated grain boundaries in this figure are the evidence for the occurrence of the second stage DRX in the region R3.

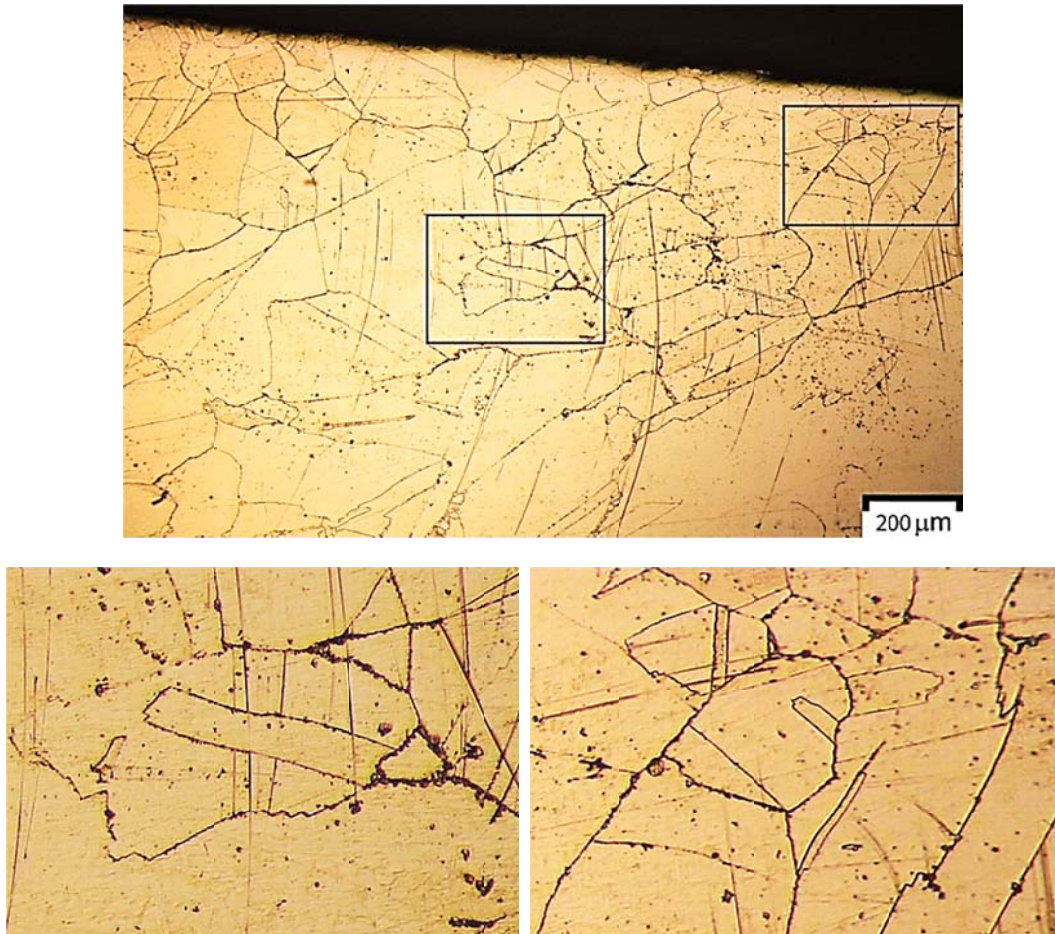


Fig. 5. Microstructure of region R4 of sample A1 with the deformed twins.

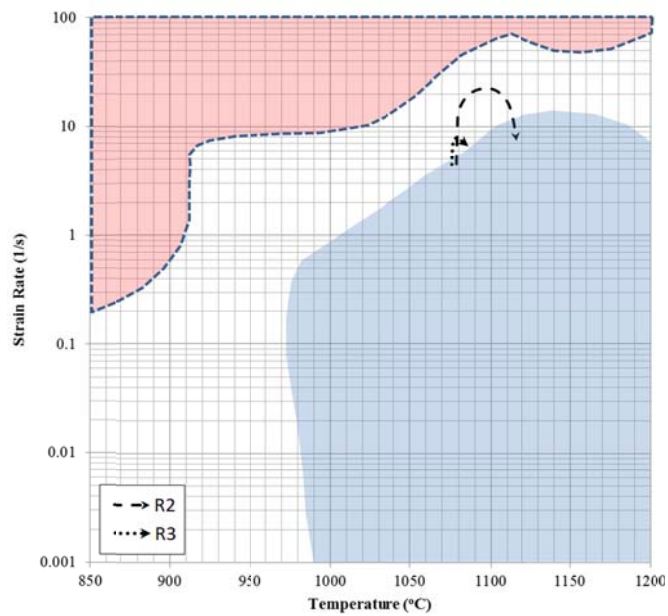


Fig. 6. Variation of strain rate vs. temperature for regions R2 and R3 of sample A1. Arrows shows the deformation directions.

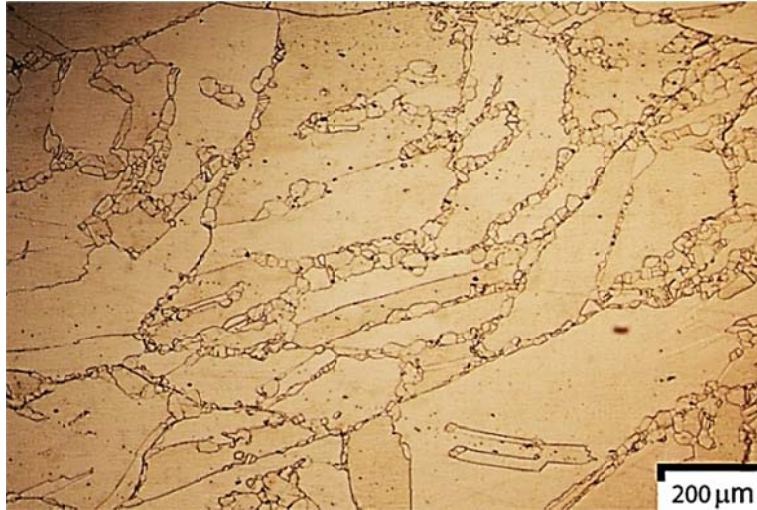


Fig. 7. Microstructure of region R2 of sample A1.

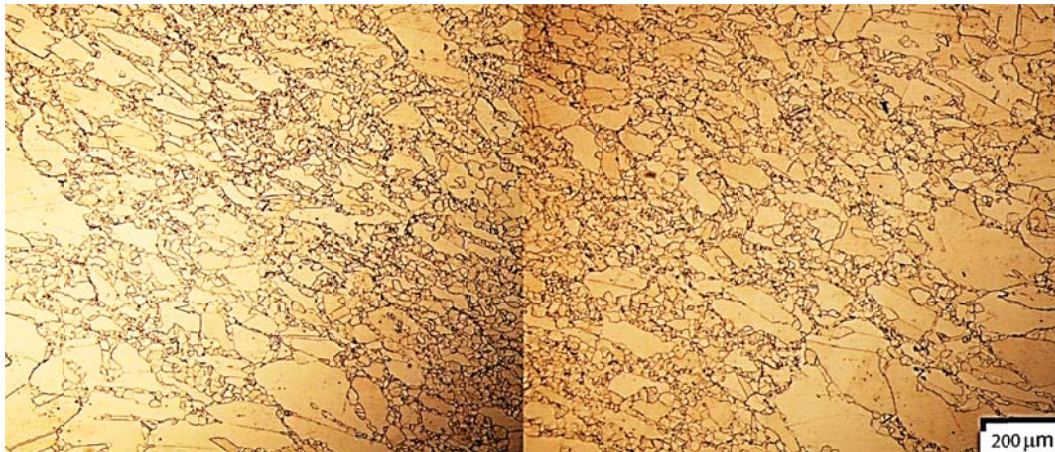


Fig. 8. Microstructure of region R3 of sample A1.

4.2. Sample A2

In order to study the effects of forging inter passes heating on the alloy microstructure, the A1 sample are preheated at 1175 °C for 5 minutes (referred as sample A2). By heating the deformed material at high temperature, depending on the deformed microstructure, different metallurgical phenomena such as static and meta-dynamic recrystallization and grain growth may happen. The microstructure of sample A2 in different regions, R1, R2, R3 and R4 are shown in Fig. 9. Comparing Figs. 9a and 9d to the Figs. 4 and 5 respectively show that there are no especial changes in the grain structure of regions R1 and R4 of sample A1 after preheating while the presence of equi-axed grains and annealing twins in Fig. 9b in comparison to elongated and partially recrystallized grains of Fig. 7, show that there is static or meta-dynamic recrystallization in the region R2 of sample A2. A similar trend can also be found in Fig. 9c, for region R3. While static recrystallization is prominent in region R2 of sample A2, the meta-dynamic recrystallization and growth of recrystallized grains are more prominent in region R3.

4.3. Sample A3

The equivalent strain of the second stage forging of sample A3 calculated by FEM analysis for regions R1, R2, R3 and R4 are 0.05, 0.86, 0.65, and 0.76 respectively. According to the equivalent strain distribution, region R1 has small strain value while other regions of deforming sample have sufficient plastic strain for DRX. In Fig.10, the variation of strain rate vs. temperature during the second stage forging of sample A3

is shown on the material processing map for regions R2, R3 and R4. From Fig. 10, it is deduced that at the beginning of the second stage forging of sample A3, temperature and strain rate are not appropriate for DRX. In fact, strain rate is higher than that of DRX range, and equivalent strain have small value at the beginning of the deformation. However, at the end of press stroke due to the decrease in the ram velocity (Fig. 1), the strain rate in the deforming material is decreased. The temperature of regions R2 and R3 are increased because of deformation heating, while due to die chilling effect, temperature of region R4 is decreased. Hence, the thermo-mechanical condition will be suitable for DRX in the regions R2 and R3, and it is expected that sample A3 have deformed grains and some evidence of DRX at the grain boundaries of regions R2 and R3, which results from the deformation condition at the end of press stroke. Fig. 11 shows the microstructure of region R3 of sample A3. Comparing this figure to Fig. 9c, it is concluded that during the second stage of forging, grains are elongated, and in the higher magnification, some evidence of serration and very fine grains on the deformed grain boundaries are found, which shows the beginning stages of DRX formation.

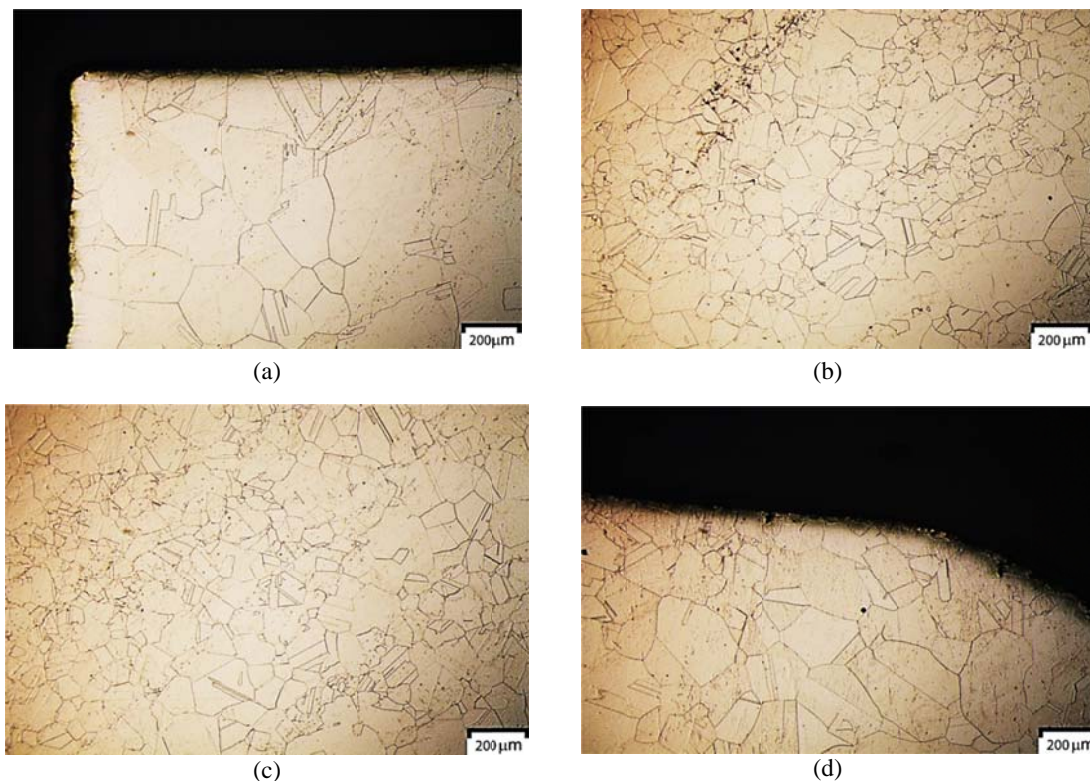


Fig. 9. Microstructure of different regions of sample A2, (a) region R1, (b) region R2, (c) region R3 and (d) region R4.

4.4. Sample A4

In order to investigate the effect of deformation path on the microstructure, the results obtained from the two steps forging (sample A3) are compared to that of single step forging (sample A4). According to the FEM simulation results, in the sample A4, the equivalent strain of regions R1, R2, R3 and R4, are 0.08, 1.81, 0.91 and 0.95 respectively. In the R1 region due to the temperature losses caused by the contact with die and small deformation, there is no DRX (Fig. 12). In the Fig.13, the variation of strain rate vs. temperature for regions R2, R3 and R4 of sample A4 are shown on the material processing map. According to Fig. 13, the initial strain rate in the regions R2 and R3 is very high that is because of location of these regions on the X pattern of strain rate, and also the high velocity of pressing die as approaching the material (Fig. 1). Therefore, DRX is suppressed in the early stages of deformation, and large plastic

strain is accumulated in these regions of material. As deformation proceeds, pressing die velocity and strain rate is decreased, and the condition will be suitable for DRX which causes the formation of fine recrystallized grains in the material. Microstructure of region R2 of sample A4 is shown in Fig. 14. From this figure it can be said that the microstructure are partially recrystallized and new grains are found on the elongated and deformed grains. According to the processing map of Fig. 13, during deformation, the region R4 of sample A4 is in the region of adiabatic shear band formation. Therefore, the flow instability expected to be occurred in region R4 of the material. The microstructure of this region of sample A4 is shown in Fig. 15, which is depicted a recrystallized grain structure along with the presence of adiabatic shear bands with very fine grains. At higher magnification, severe flow localization on the shear bands can be seen (Fig. 15b). However, there is no such visible shear bands in the sample forged at the two steps due to the lower strain rate.

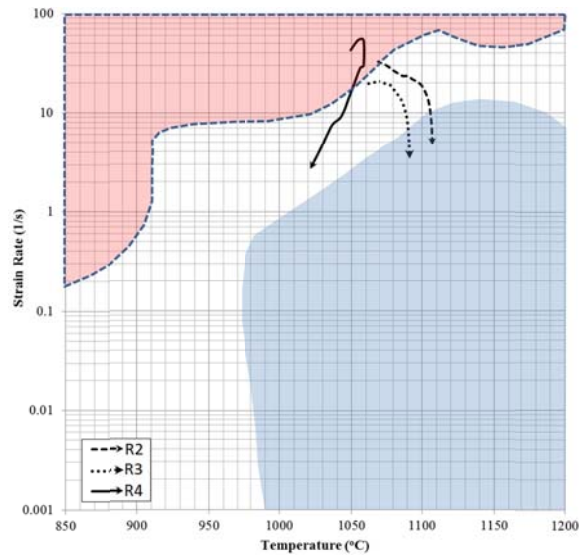


Fig. 10. Variation of strain rate vs. temperature for different regions of sample A3, during the second stage forging. Arrows show deformation directions.

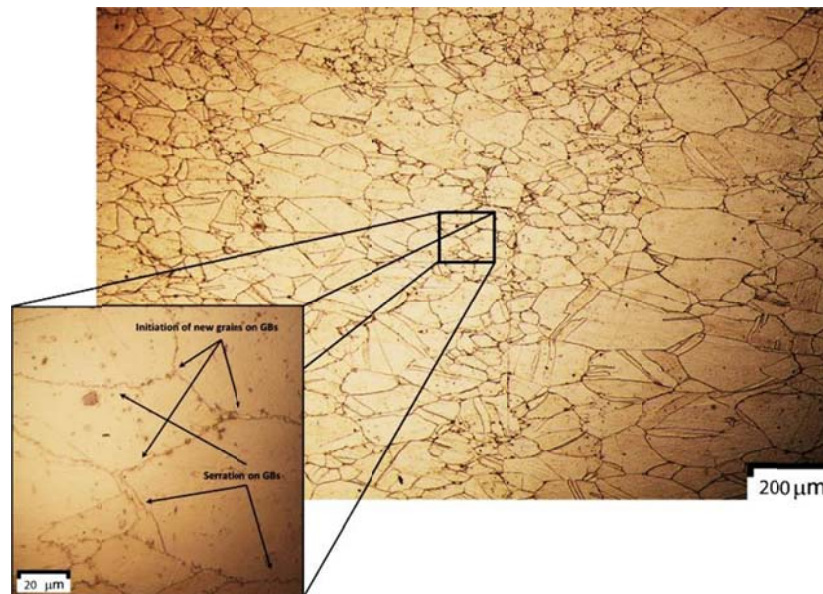


Fig. 11. Microstructure of region R3 of sample A3.

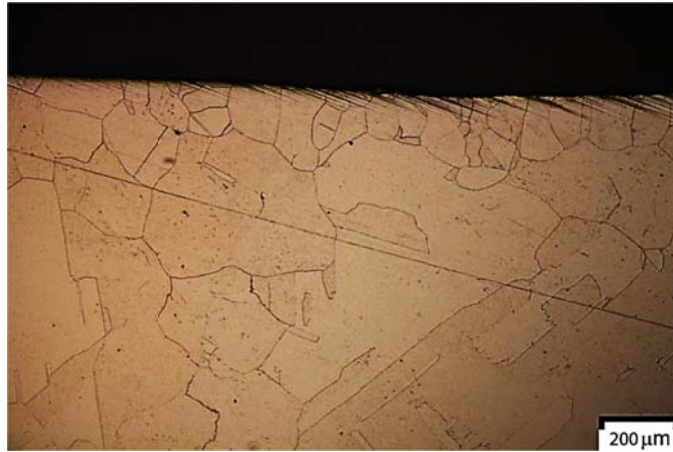


Fig. 12. Microstructure of region R1 of sample A4.

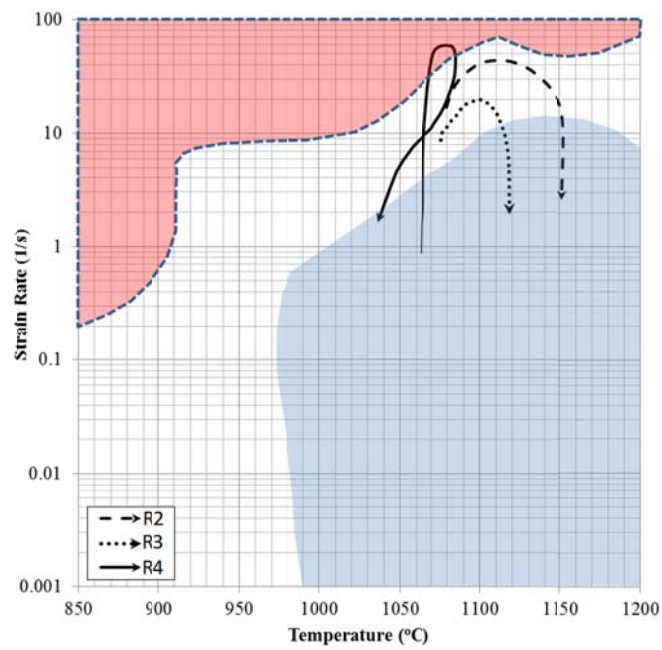


Fig. 13. Variation of strain rate vs. temperature for different regions of sample A4, arrows show deformation directions.

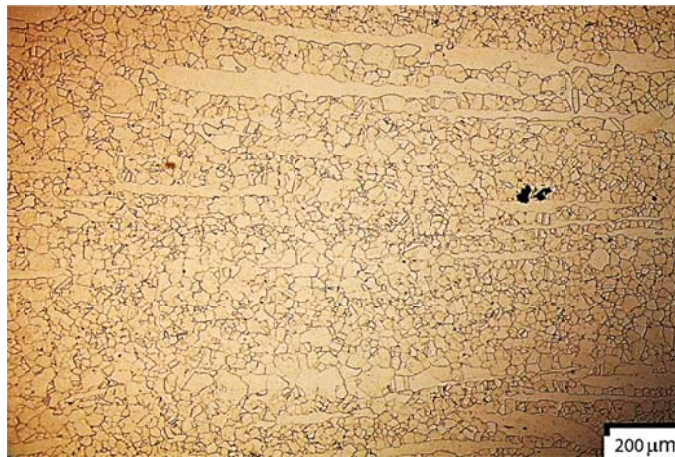


Fig. 14. Microstructure of region R2 of sample A4.

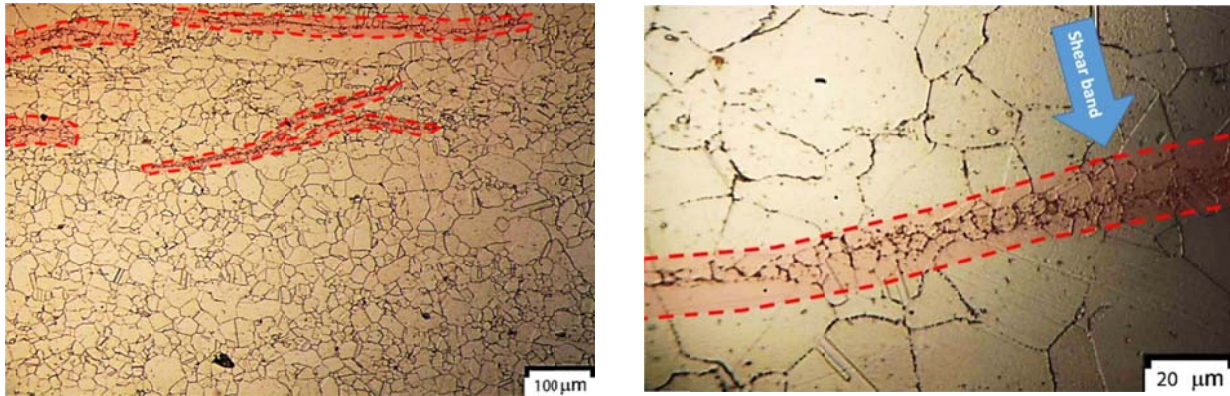


Fig. 15. Microstructure of region R4 of sample A4 (shear bands are shown with dashed lines).

5. Conclusion

Hot deformation behavior of Nimonic 80A alloy as a material for gas turbine blades was studied via non-isothermal side pressing test. The results obtained from the finite element analysis, microscopy observation and the alloy processing map, are as follows:

The distribution of deformation parameters (i.e. strain, strain rate, and temperature) are non-uniform in the deforming sample cross section. The X like pattern is formed in the cross section with the higher values of deformation parameter along this pattern, while other parts of the cross section have lower values. If the severity of this non-uniformity which depends on the amount of sample reduction in each pressing stroke is high, flow localization can be caused. By performing forging in one step, the non-uniform dynamic recrystallization happened due to a very high and localized strain rate and heat of deformation, which causes the formation of adiabatic shear bands while performing forging in the two steps, results in uniform distribution of deformation parameters and thus the dynamic recrystallization occurred uniformly. Therefore, performing forging in the two steps from the microstructural view has the better final microstructure and hot workability and thus preferred.

Acknowledgement: One of the authors (R.M) would like to acknowledge the Turbine machine Middle East Co. for providing the research facilities used in this work.

5. References

- [1] D. Bombac, M. T. Fazarinc and S. V. Goran KuGler, Microstructure development of Nimonic 80A superalloy during hot deformation, *Materials and Geoenvironment*, 55 (2008) 319-328.
- [2] D. Bombac, M. Brojan, M. Tercelj and R. Turk, Response to hot deformation conditions and microstructure development of Nimonic 80A superalloy. *Materials and Manufacturing Processes*, 24 (2009), 644-648.
- [3] S. Kargarnejad and F. Djavanroodi, Failure assessment of Nimonic 80A gas turbine blade. *Engineering Failure Analysis*, 26 (2012), 211-219.
- [4] T. M. Pollock and S. Tin, Nickel-based superalloys for advanced turbine engines: chemistry, microstructure and properties. *Journal of propulsion and power*, 22(2) (2006), 361-374.
- [5] G. Tai, Y. He and L. Yu-li, Backward tracing simulation of precision forging process for blade based on 3D FEM. *Trans. Nonferrous Met. Soc. China*, 16 (2006), 639-644.
- [6] S. L. Semiatin and J.J. Jonas, *Formability and Workability of Metals*, IV (1984), Ohio: American Society for Metals.
- [7] G. E. Dieter, *Evaluation of Workability*. (1990), University of Maryland.

- [8] A. R. Mashreghi, H. Monajatizadeh, M. Jahazi and S. Yue, High temperature deformation of nickel base superalloy Udimet 520. *Materials Science and Technology*, (2004), 161-166.
- [9] Z. M. Hu, J.W. Brooks and T.A. Dean, Experimental and theoretical analysis of deformation and microstructural evolution in the hot die forging of titanium alloy aerofoil sections. *Journal of Materials Processing Technology*, 88 (1999), 251-265.
- [10] R. S. Lee and H.C. Lin, Process design based on the deformation mechanism for the non-isothermal forging of Ti-6Al-4V alloy. *Journal of Materials Processing Technology*, 79 (1998), 224-235.
- [11] Y. Prasad and S. Sasidhara, *Hot Working Guide: A Compendium of Processing Maps*, (1997), ASM international.
- [12] L. U. Shi-qiang, L. Xin, K. L. Wang, L. Shi-biao and M. W. FU, A method for prediction of unstable deformation in hot forging process by simulation. *Transactions of Nonferrous Metals Society of China*, 23(12) (2013), 3739-3747.
- [13] N. Srinivasa and Y. Prasad, Hot working characteristics of nimonic 75, 80A and 90 superalloys: a comparison using processing maps. *Journal of Materials Processing Technology*, 51(1) (1995), 171-192.